

We are IntechOpen, the world's leading publisher of Open Access books Built by scientists, for scientists

6,900

Open access books available

186,000

International authors and editors

200M

Downloads

Our authors are among the

154

Countries delivered to

TOP 1%

most cited scientists

12.2%

Contributors from top 500 universities



WEB OF SCIENCE™

Selection of our books indexed in the Book Citation Index
in Web of Science™ Core Collection (BKCI)

Interested in publishing with us?
Contact book.department@intechopen.com

Numbers displayed above are based on latest data collected.
For more information visit www.intechopen.com



Mg-Based Quasicrystals

Zhifeng Wang and Weimin Zhao

Additional information is available at the end of the chapter

<http://dx.doi.org/10.5772/48163>

1. Introduction

Quasicrystals (QCs) are a well-defined ordered phase of solid matter with long-range quasi-periodic translational order and an orientational order [1], but no three dimensional translational periodicity [2]. In 1984, Shechtman et al [3] first reported these structures in a rapidly solidified Al–Mn alloy. It brings about a paradigm shift in solid-state physics for these atomic arrangements are forbidden for conventional crystallography [4] and have long been thought forbidden in nature. The unexpected discovery of QCs presents scientists with a new, puzzling class of materials and involves hundreds of researchers in this realm. During the beginning period for QC study, many QCs were fabricated in Al-based alloys [5]. Luo et al [6] discovered first Mg-based QCs in Mg–Zn–(Y, RE) system in 1993 which extend the alloy system of QCs.

So far, QCs in various systems have been synthesized in laboratories [2] and have also been discovered in a natural mineral [7] which comes from extraterrestrials. Many noticeable results were disclosed. The reported evidence [8] indicates that QCs can form naturally under astrophysical conditions and remain stable over cosmic timescales, giving unique insights on their existence in nature and stability. In 2011, the Nobel Prize in Chemistry was awarded to Daniel Shechtman for “the discovery of quasicrystals”. Nowadays, scientists all over the world refocus these amazing materials and their promising applications.

As is well-known, QCs possess a host of unusual mechanical and physical properties [9] such as high strength, high thermal conductivity, and low friction coefficient [10]. Though they cannot be applied directly as structural materials for their innate brittleness, they can be used as good strengthening phases for some flexible matrix. Moreover, QCs have good corrosion resistance and were introduced into compounds which have been applied in some medical fields [11,12]. In this chapter, QC morphology evolution, its influence factors, QC-

strengthened alloys and QC corrosion resistance are discussed. These basic researches are very useful for further development of QCs.

2. Morphologies of quasicrystals

QCs present fascinating three dimensional morphologies such as dodecahedral and icosahedral shapes (Fig.1). In different alloy systems, QC can be produced by slow-cooling method or rapidly solidified method. Mg-Zn-Y QCs possess a broad QC forming range. They can be synthesized in a common casting process [10].

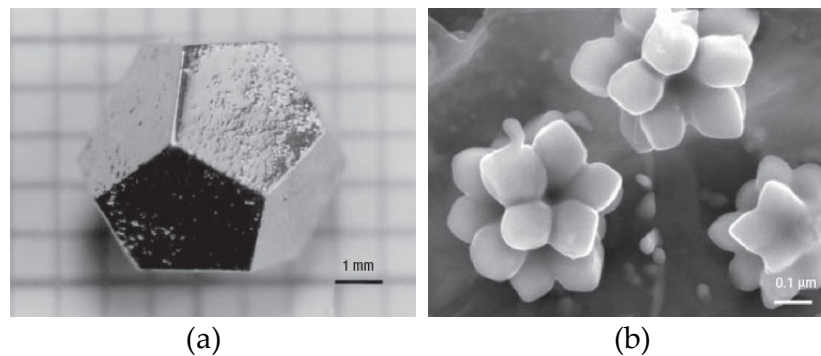


Figure 1. Fascinating quasicrystals [13] (a) Dodecahedral Zn-Mg-Ho single QC grain (b) Icosahedral Al-Mn QC flowers

2.1. Morphology evolutions of Mg-Zn-Y quasicrystals [14]

The $Mg_{72}Zn_{26.5}Y_{1.5}$ (at.%) alloys were produced by a reformed crucible electric resistance furnace (SG₂-5-10A, as shown in Fig.2), melted under the mixture of SF₆/CO₂ protective atmosphere. Stirring for 2 min by impellor at 1073K and holding for 5 min above 1053K, the melt was poured and cooled by different cooling media (as shown in Fig.3 and Table 1). The cooling curves (as shown in Fig.4) of the alloys were monitored by multichannel data acquisition cards. The results showed that, the cooling rate was sequentially decreased from cooling media 1 to 5. The SEM images of Alloy 1 ~ Alloy 5 were shown in Fig.5.

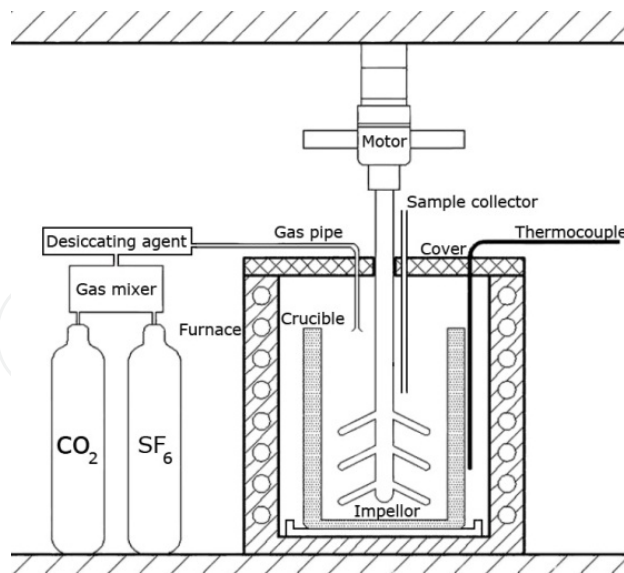


Figure 2. Schematic diagram of apparatus for making QC alloys

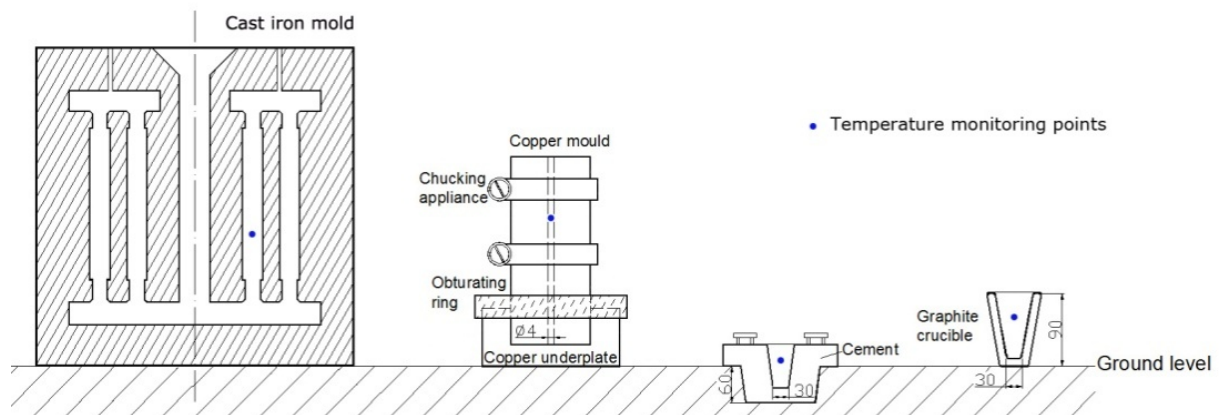


Figure 3. Schematic diagram of cooling media

Alloy no.	Cooling
1	Be extracted by sample collector and cooled in water
2	Copper mould
3	Cast iron mould
4	Cement mould
5	Be poured into a graphite crucible and cooled in air

Table 1. Cooling media of the alloys

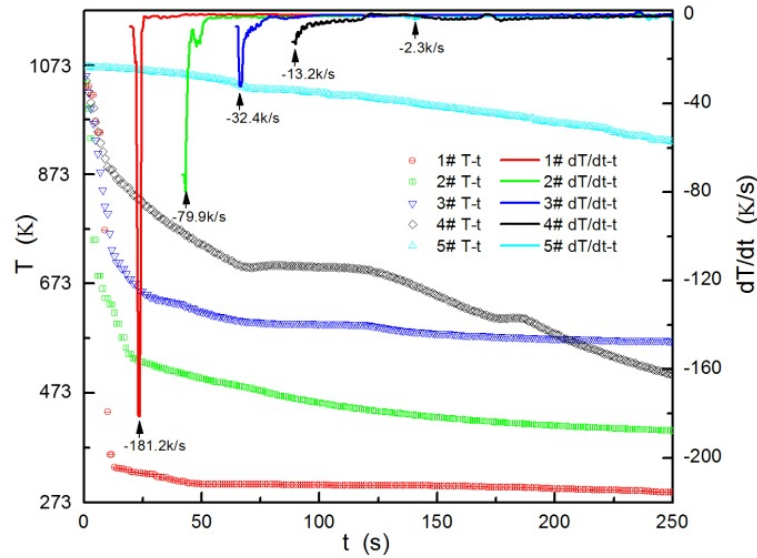


Figure 4. Cooling curves of the Alloys

The QC size gradually increased and the QC morphology changed with decreasing cooling rate. Decahedral quasicrystals (DQCs) were formed in Alloy 1 under cooling media 1, while icosahedral quasicrystals (IQCs) were formed in Alloy 2 ~ Alloy 5 under other cooling media. Moreover, the microhardness was larger for the smaller-sized QCs (Table 2). IQCs are quasiperiodic in three dimensions, while DQCs are quasiperiodic in two dimensions [2]. The DQCs formed in Alloy 1 presented flat bacilliform morphology and 10-fold symmetry characteristic. With decreasing cooling rate, the IQCs in Alloy 2 and Alloy 3 exhibited petal-like morphology under metal mould casting condition. Furthermore, the slower cooling rate induced larger IQC petals. With the further decrease of the cooling rate, the IQC petals showed nearly circular morphology. Finally, the IQCs grew up to large polygons in the slow cooling conditions.

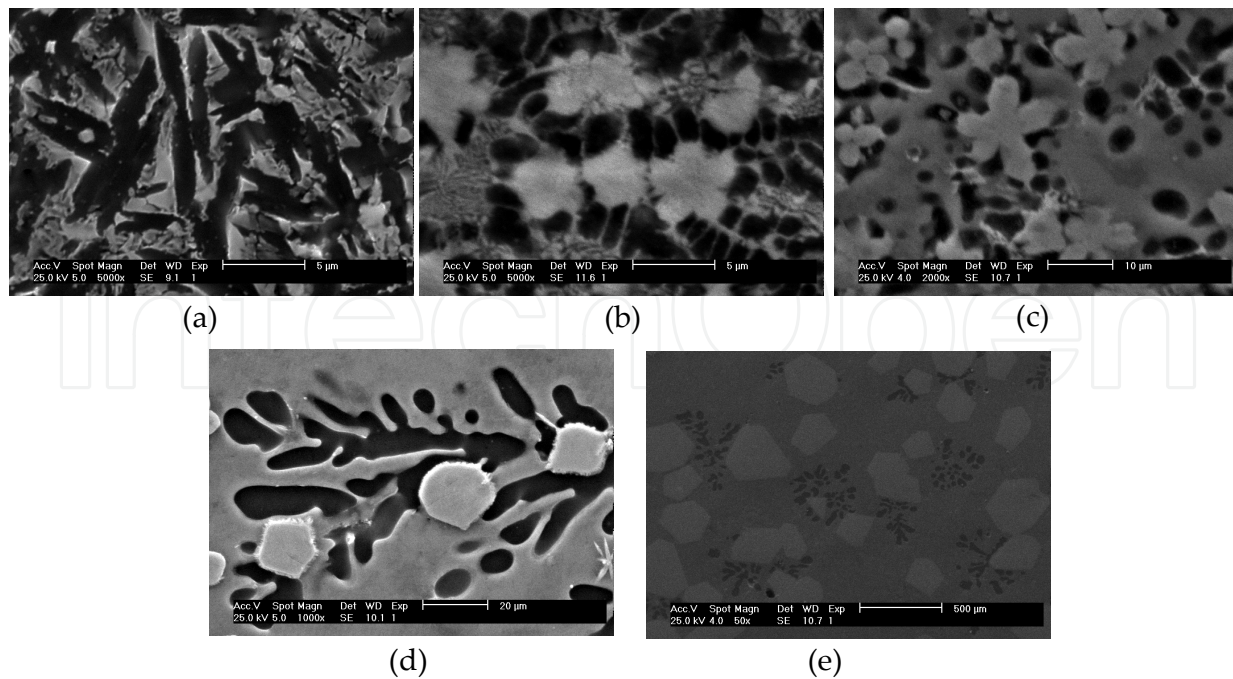


Figure 5. SEM images of Alloy 1~5 a) Alloy 1 (b) Alloy 2 (c) Alloy 3 (d) Alloy 4 (e) Alloy 5

Alloy no.	QC size / μm	QC morphology	QC microhardness / HV
1	10~12 in length	Flat X-shape	287
2	4~6	Petal-like	272
3	10~15	Petal-like	157
4	18~22	Near circular petal-like	182
5	300~400	Polygon	195

Table 2. Comparisons of the quasicrystals

In order to clarify how the IQCs transformed from morphology of Alloy 1 to Alloy 2, the $\text{Mg}_{72}\text{Zn}_{26}\text{Y}_{1.5}\text{Cu}_{0.5}$ alloys were synthesized under a water-cooled copper mold with pouring gate diameter of 2 mm and 4 mm. Such cooling rates were just between the cooling media 1 and 2. The cooling rate of water-cooled copper mold with pouring gate diameter of 2mm was faster than that of 4mm. Flat DQCs like Alloy 1, and spherical IQCs were formed respectively in Fig.6 (a) and (b), and pouring gate diameter was 2mm and 4mm correspondingly. We can see from Fig.6, a plane branch grew out in one of two-dimensional (2D) prior growth directions of the flat DQCs (marked by a red arrow in Fig.6 (a)). And then more branches grew out in three-dimensional (3D) directions (marked by a red arrow in Fig.6 (b)). These branches increasingly became dense and agglomerate, and finally created a cluster for the primary IQC morphology.

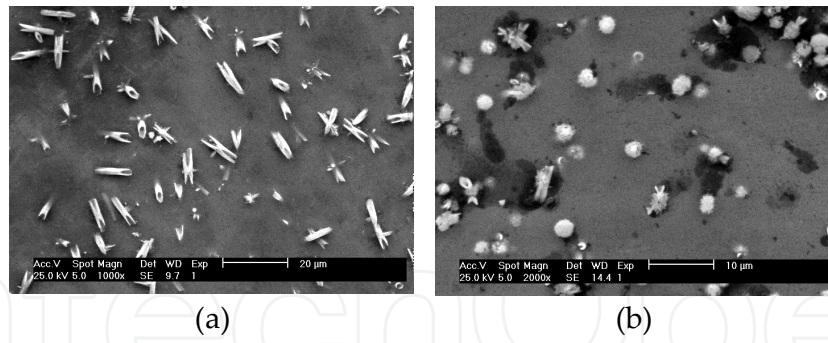


Figure 6. SEM images of $Mg_{72}Zn_{26}Y_{1.5}Cu_{0.5}$ alloys (a) Flat DQC (b) Spherical IQC

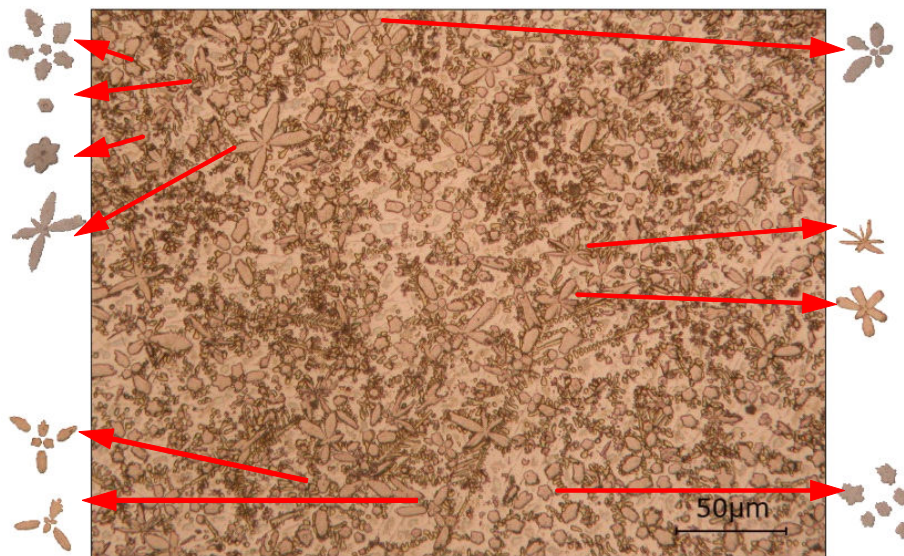


Figure 7. Optical microstructure of Alloy 3 after heat treatment at 750 K for 15 min

A heat treatment for Alloy 3 at 750 K for 15 min was prepared for studying IQC growth process between IQC morphology in Alloy 3 and in Alloy 4. It can be seen from Fig.7 that various shapes of QCs at different growth stages were formed in the heat treatment process. There were plentiful IQC nuclei in as-cast Alloy 3, but the growth was not complete due to a fast cooling process. The petals shown in Alloy 3 were the ones who had experienced the nucleation process only, but do not have enough time to grow up into the morphology in Alloy 4. During the heat treatment, the IQC nuclei continued to grow.

From the above, the IQC morphology evolution process between IQCs in Alloy 1 and Alloy 2 as well as between IQCs in Alloy 3 and Alloy 4 were revealed. A general drawing of morphology evolution of Mg-Zn-Y quasicrystal phase in growth process was shown in Fig.8. Twenty-two kinds of typical morphology of Mg-Zn-Y QC phase during cooling process were extracted from SEM and OM images.

During cooling process of Mg-Zn-Y alloys, at first a plane branch (shape 2) grew out in one of prior growth directions of the flat DQCs (shape 1). And then more branches emerged and created a cluster (shape 3), which was the primary morphology of IQCs. At the beginning of the IQC growth stage, its morphology was near spherical (shape 4). The spherical interface was not maintained with alteration of the ambience conditions. Along the prior growth directions, the spherical IQC sprouted five petals (shape 5) or six petals (shape 16). These petals subsequently grew up and became larger in length (shape 6 and shape 17), and further separated from each other (shape 8 and shape 18). The separated IQC petals grew up (shape 9) and became new independent IQCs (as shape 5). If there were still leftover Zn and Y elements in the melt, the IQC petals will continue to split and repeat the cycle from shape 5 to shape 9 until they were used up. With decrease of the cooling rate and increase of the growth time, the IQCs became maturity and grew bigger (shape 11), and finally grew into bulk polygons (shape 12 and 13).

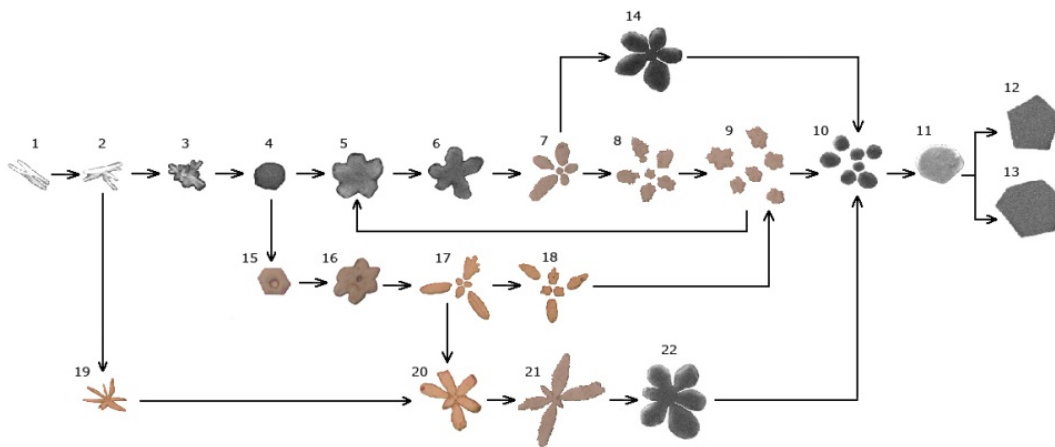


Figure 8. Schematic diagram of morphology evolution of Mg-Zn-Y quasicrystal phase in growth process

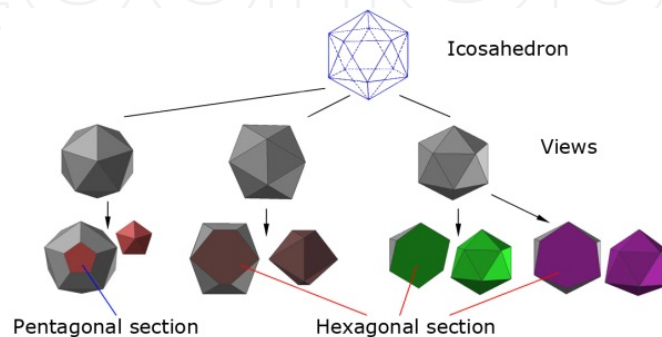


Figure 9. Section schematic diagram of icosahedrons

The reason why the final morphology of IQCs was pentagonal (shape 12) and hexagonal (shape 13) polygon can be showed in Fig.9: a mature Mg-Zn-Y quasicrystal is an icosahedron in a 3-D view; when we observe it in different directions, it show different views; and when we grind and polish samples in parallel direction to the views, pentagonal and hexagonal cross-section morphology are presented with multiple probability.

2.2. Effects of the fourth component and undercooling [15,16]

The solidified process of quasicrystal phases which consist of grain nucleation and subsequent growth is similar to crystals. It was necessary to properly control the cooling rate during these two processes for the formation of the quasicrystal phase is thermodynamically unstable. Lower cooling rate might not effectively suppress the crystallization and would result in the formation of crystal phase while higher cooling rate might suppress the nucleation and growth of the quasicrystal phase and would result in the formation of amorphous phase. For quasicrystal containing magnesium alloys, stable icosahedral quasicrystal phase (I-phase) can be obtained under normal casting conditions.

At the early stage of nucleation process, the single fourth component particles act as potential nucleating substrates, and the morphology of I-phase should be nearly spherical. Because the coalescence of the fourth component at solidification front, surface energy at that local region was elevated, and growing velocity of I-phase slowed down. Moreover, the same heat dissipating condition in all directions leads to the same growing velocity of I-phase in all directions. Furthermore, during this process, highest volume percentage of surface layer to the whole volume of I-phase particle resulted in highest surface energy of I-phase, which enabled the morphology of I-phase particle shrinking to spherical or near-spherical. Therefore, the solidified morphology of I-phase depended on the stability of spherical I-phase during the subsequent growth [17]. I-phase with spherical morphology would be obtained if I-phase forming initially could preserve spherical interface stable in the whole growth process. Otherwise, I-phase with irregular or dendrite morphology would be eventually generated. According to the research results of Mullins et al. [18], relative stability criterion of spherical interface with radius being R_r can be expressed by the rate of change per unit perturbation amplitude:

$$\frac{\dot{\delta}}{\delta} \leq \frac{\dot{R}}{R} \quad (1)$$

$$\frac{\dot{\delta}}{\delta} = \frac{(l-1)K_l}{K_s L} \left[\Delta T - \Gamma \frac{T_m \Gamma}{R} (1 + \partial_t) \right] \quad (2)$$

The critical radius maintaining the spherical I-phase interface relative stable was:

$$R_r = \frac{2T_m \Gamma}{\Delta T} \left[1 + \frac{(l-1)}{(l-2)} \partial_t \right] \quad (3)$$

$$\delta_t = \frac{1}{2}(l+2) \left[1 + l \left(1 + \frac{K_s}{K_l} \right) \right] \quad (4)$$

Where δ is the amplitude of fluctuation, K_s the thermal conductivity of the solid phase, K_l the thermal conductivity of the liquid phase, L is latent heat of freezing, ΔT is degree of undercooling in the melt, Γ the ratio of interface energy to latent heat of solid phase per unit volume, l the rank of spherical harmonic function, T_m is the melting point of the alloy.

It can be known from Eqs. (3)~(4) that decreasing ΔT or elevating the interface energy between the I-phase and the melt were beneficial to the stability of spherical interface. The addition of a certain amount of the fourth component not only provided potential nucleating sites for I-phase, but also purified the melt by removing oxygen and the fourth component with harmful impurity elements. The coalescence of the fourth component compounds at solid/liquid interface resulted in higher interface energy and higher value of Γ . Moreover, the addition of the fourth component promoted heterogeneous nucleation of I-phase, lowered the degree of undercooling ΔT and increased the critical radius R_c . Meanwhile, the same heat dissipating condition of the I-phase particle in all directions resulted in the same growing velocity of I-phase particle in all directions, enabling I-phase to keep spherical growing front and providing positive conditions for spherical growth of I-phase.

However, if superfluous addition of the fourth component, un-dissolved fourth component will discharge from the solid phase to solid/liquid interface and formed the fourth component solute transitional layer with certain thickness. Moreover, due to the increasingly enrichment of the fourth component compounds in front of the growing solid/liquid interface of I-phase particle, the degree of constitutional under-cooling increased, and ΔT increased as well.

$$\Delta T = \Delta T_h + \Delta T_c + \Delta T_k \quad (5)$$

Where ΔT_h is thermodynamics undercooling, ΔT_c the constitutional undercooling, and ΔT_k the kinetics undercooling. It means that ΔT is composed of three parts of ΔT_h , ΔT_c and ΔT_k .

Increased ΔT intensified the instability of spherical growing surface of I-phase particle. Then the I-phase turn to coarse, the spherical morphology will be wrecked and transform to petal-like.

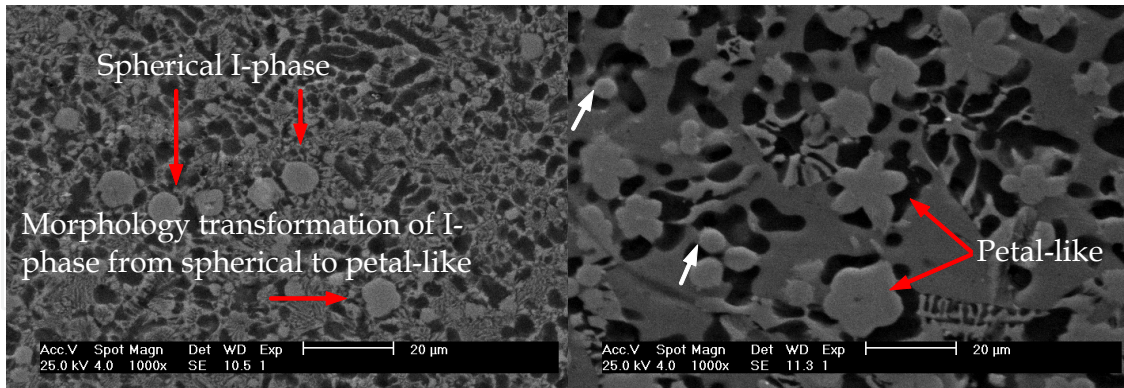


Figure 10. SEM images of as-cast Mg-Zn-Y-Sb alloys containing I-phase; (a) $Mg_{72.2}Zn_{26.2}Y_{1.5}Sb_{0.1}$ (b) $Mg_{72.1}Zn_{26.2}Y_{1.5}Sb_{0.2}$

Fig.10 shows SEM images of Mg-Zn-Y-Sb alloys. I-phase morphology in $Mg_{72.2}Zn_{26.2}Y_{1.5}Sb_{0.1}$ was spherical while $Mg_{72.1}Zn_{26.2}Y_{1.5}Sb_{0.2}$ presented petal-like. It can be seen from Fig.10(a) that the value of critical radius R_c of I-phase in Mg-Zn-Y-0.1Sb alloy was about $8\mu m$ when the content of the fourth component Sb was 0.1%. If local conditions changed, and spherical radius value exceed R_c , the morphology transformation of I-phase from spherical to petal-like will be occurred (marked by the lower red arrow in Fig.10(a)). So we can see that the superfluous addition of the fourth component was negative to the stability of spherical interface, and also made against to forming spherical I-phase. We can see from Fig.10(b): most parts of I-phase are petal-like while a few of I-phase are spherical(marked by white arrows). Therefore a critical stable radius indeed exists. Once the interface radius of I-phase is larger than R_c in IQC growth process, the final morphology of I-phase in that local zone will be petal-like. Conversely, spherical morphology will be preserved in local zone if the interface radius of I-phase is smaller than R_c .

The effect of different contents of the fourth component and different degree of undercooling on critical stable radius of spherical I-phase can be shown in Fig.11. As we discussed above, for certain cooling conditions and certain compositions of Mg-Zn-Y alloys, certain size of critical stable radius exist and we describe this state as state I. The addition of a small amount of the fourth component is able to result in an decrease of degree of undercooling and finally increase the critical stable radius R_c as seen in Eqs.(3). We can describe this state as state II. However, if superfluous addition of the fourth component, constitutional undercooling will come out, ΔT will increase. Thus the critical stable radius of spherical I-phase will decrease. This state can be called state III.

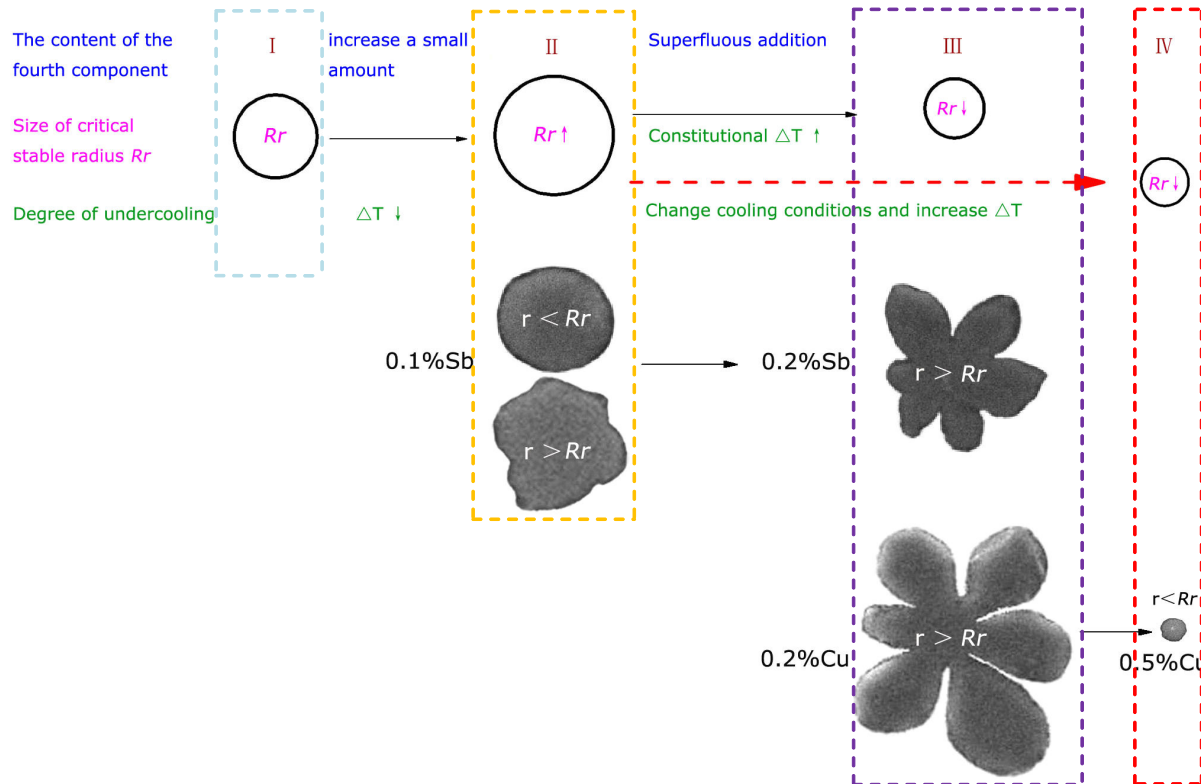


Figure 11. Schematic diagram of different states and transform process of critical stable radius

For a certain cooling condition and a certain composition of alloys, different contents of the fourth component and their critical stable radius have relationships of one-to-one correspondence. Fig.11 takes the fourth component Sb and Cu for examples. Only when the radius of IQC less than R_r in their respective states can spherical IQC be formed. Under most of the conditions, if superfluous addition of the fourth component, small-sized R_r will generate big-sized petal-like IQC. It seems as if superfluous addition of the fourth component could not produce spherical I-phase. Actually, we can improve cooling conditions and increase ΔT_h and ΔT artificially. Much smaller critical stable radius will make it difficult to forming spherical I-phase. However, higher cooling rate might cut down the growth time of the quasicrystal phase. Spherical interface of I-phase forming preliminary stage will be stably preserved in the whole growth process, and then smaller-sized spherical I-phase which its radius less than R_r will occurred. We can define this state as state IV. Under these principles, a kind of spherical I-phase with high content of the fourth component but amazing minisize (as shown in Fig.12(b)) can be produced by using a water-cooled copper mould (as shown in Fig.13(a)). So, it is a novel way to produce spherical I-phase with high content of the fourth component in minisize by increasing thermodynamics undercooling artificially. In this way, we can easily control cooling rate in a certain range and obtain quaternary spherical IQC with different minisize scale.

Searching proper content of different fourth component, confirming the size of spherical stable radius, developing quaternary spherical IQC with different minisize scale, and thoroughly making good use of IQC particles as reinforcement phase are future problems and proper research points.

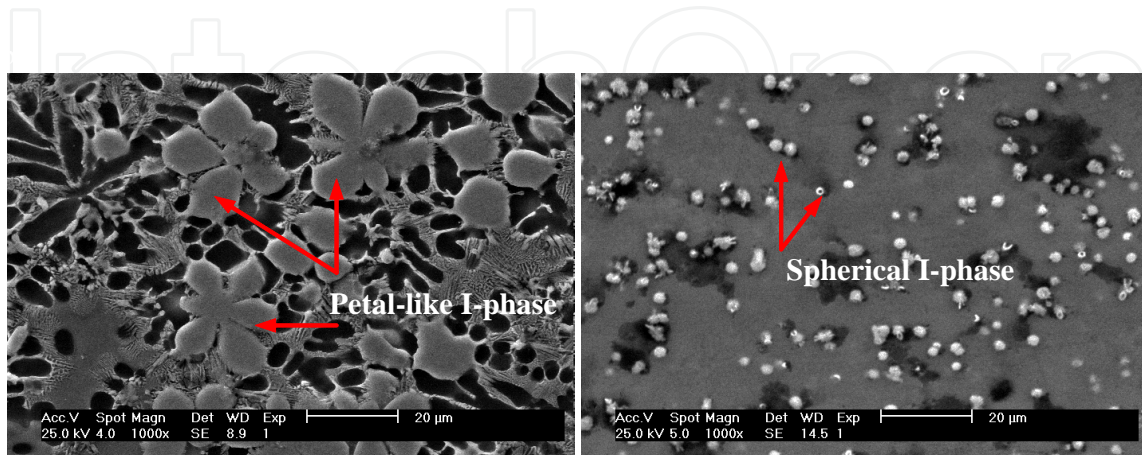


Figure 12. SEM images of Mg-Zn-Y-Cu alloys cooled in different mould (a) $Mg_{72.1}Zn_{26.2}Y_{1.5}Cu_{0.2}$ (cast iron mould) (b) $Mg_{72.0}Zn_{26.0}Y_{1.5}Cu_{0.5}$ (water-cooled Cu mould)

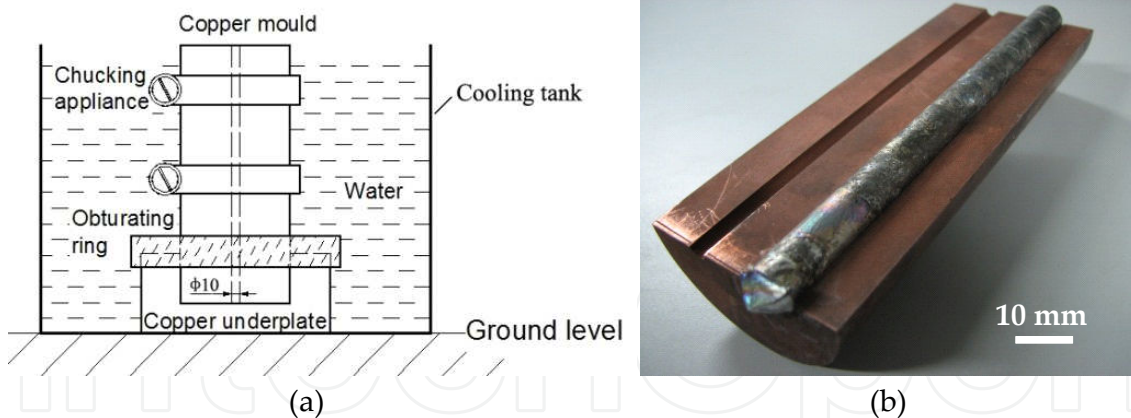


Figure 13. Mould for produces spherical QC alloys; (a) Water-cooled cooper mould (b) Casting

3. Effects of quasicrystal alloys on mechanical properties of magnesium alloys [19]

The effects of different Ce contents on microstructure of Mg-Zn-Y-Ce QC alloys are shown in Fig.14. Mg-Zn-Y QCs showed petal-like morphology under cast iron mould cooling con-

ditions. When the added Ce content was small (0.2 at.%), the morphology and size of QC petals were basically unchanged. With the increase of Ce content (0.5 at.%), the amounts and size of the QC petals were significantly increased, and the petals became more round. When the Ce content reached 0.8 at.%, the amounts of I-phases further multiplied, but the petals reduced in size. The petal branch became short, un conspicuous, and subsphaeroidal. With the further increase in Ce content (1.0 at.%), the IQC petal size grew twice that of 0.5 at.% Ce, and they were transformed as multi-secondary dendrites of the five- or six-petaled flowers. This process was in line with the cooling influencing law [15].

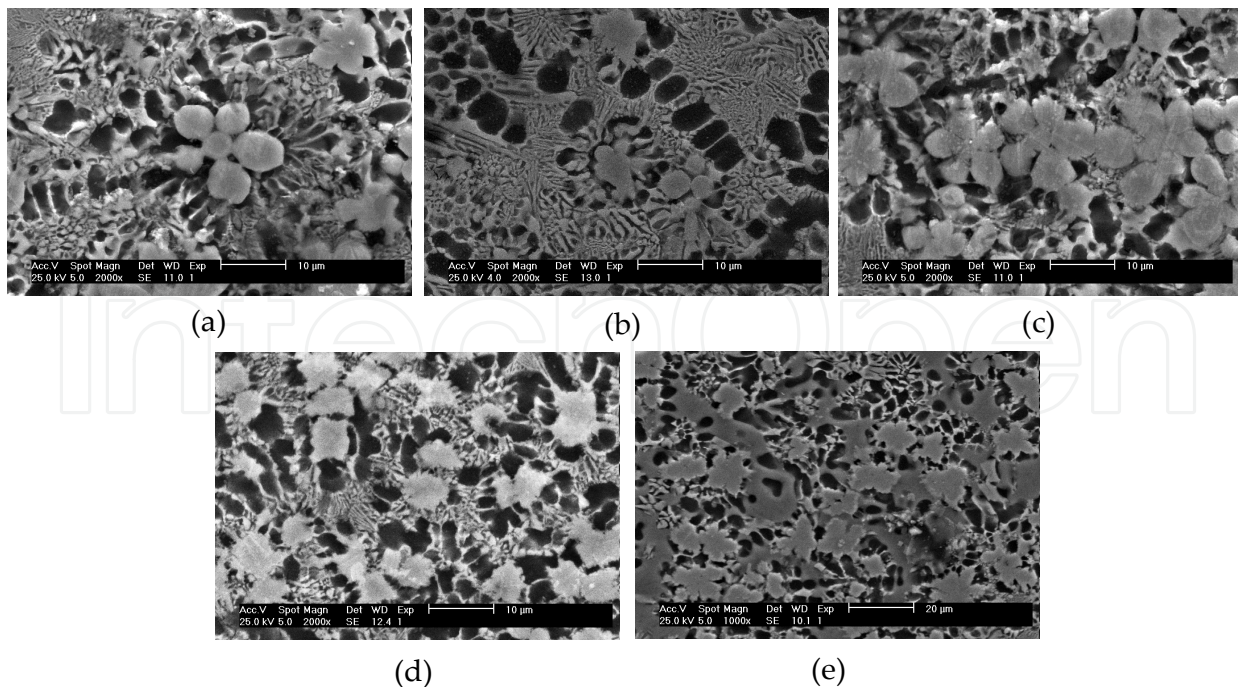


Figure 14. SEM images of the Mg-Zn-Y-Ce QC alloys. (a) $Mg_{72.5}Zn_{26}Y_{1.5}$ (b) $Mg_{72.3}Zn_{26}Y_{1.5}Ce_{0.2}$ (c) $Mg_{72.1}Zn_{25.9}Y_{1.5}Ce_{0.5}$ (d) $Mg_{72}Zn_{25.7}Y_{1.5}Ce_{0.8}$ (e) $Mg_{71.8}Zn_{25.7}Y_{1.5}Ce_{1.0}$

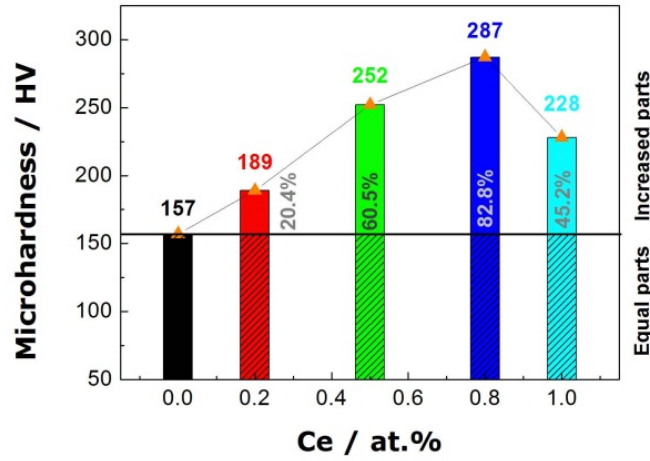


Figure 15. Microhardness of quasicrystals.

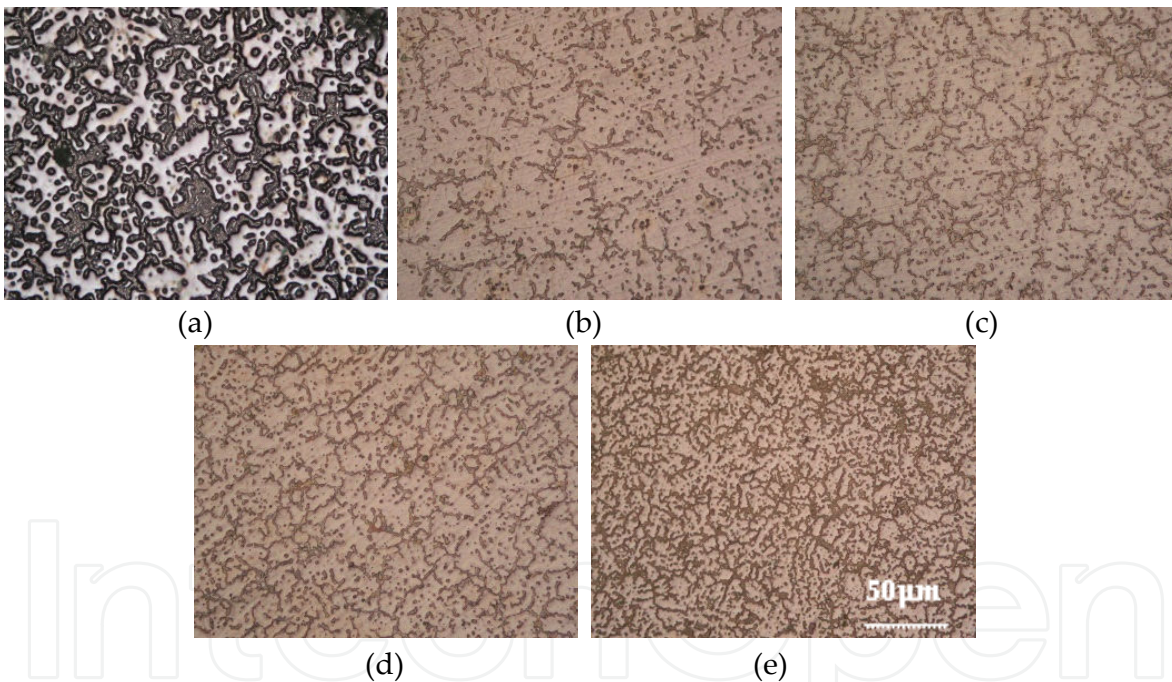


Figure 16. Microstructure of AZ91 alloys reinforced by different content of $Mg_{72}Zn_{25.7}Y_{1.5}Ce_{0.8}$ alloys (wt%). (a) 0% (b) 5% (c) 10% (d) 15% (e) 30%

The microhardness test results (as shown in Fig.15) of IQC alloys showed as the following: All values of microhardness of quaternary QCs were higher than those of ternary QCs. With increase in Ce content, the microhardness of I-phase also increased. However, when the dosage reached a certain value (i.e., 1.0%), the microhardness of I-phase decreased sharply. The microhardness value of I-phase in the $Mg_{72}Zn_{25.7}Y_{1.5}Ce_{0.8}$ alloy reached to HV287, which is 82.8% higher than that in ternary $Mg_{72.5}Zn_{26}Y_{1.5}$ alloy. In following experiments,

$Mg_{72}Zn_{25.7}Y_{1.5}Ce_{0.8}$ alloy was used as a master alloy to strengthen AZ91 alloys since the quaternary subsphaeroidal I-phase contain high microhardness and possess better wetting power with Mg matrix.

$Mg_{72}Zn_{25.7}Y_{1.5}Ce_{0.8}$ master alloys with contents of 0%, 5%, 10%, 15%, and 30% (wt.%) were added into AZ91 alloys. Changes in the microstructure of AZ91 alloys are shown in Fig. 16. With the increase in the amount of the $Mg_{72}Zn_{25.7}Y_{1.5}Ce_{0.8}$ alloy, the grains of AZ91 alloys were gradually refined, while β -phase was refined and narrowed. However, when the dosage of $Mg_{72}Zn_{25.7}Y_{1.5}Ce_{0.8}$ alloy was too high (30%), β -phase turn to coarse.

In this craft, $Mg_{72}Zn_{25.7}Y_{1.5}Ce_{0.8}$ alloy was added into molten AZ91 and remelted. In the subsequent metal mold cooling process, the I-phases nucleated, but insufficient time did not allow for the adequate increase in size. Therefore, small granular I-phases precipitated from the grain interiors of the AZ91 alloys. These granular I-phases mixed with divorced β -phase particles, which baffled the process of identification of one from the other. In several kinds of phases of $Mg_{72}Zn_{25.7}Y_{1.5}Ce_{0.8}$ alloy, only I-phases remained after remelting. Other phases integrated into the AZ91 and became constituting elements of AZ91 alloys. Since I-phases are heat-stable phases [20], they remain in the alloys and will not be broken down into other phases even in high-temperature heating process. Thus, they can play significant roles for the matrix after heat treatment. Considering this characteristic of I-phases, we can study the effects of heat treatment to further improve on the mechanical properties of QCs reinforced AZ91 alloys.

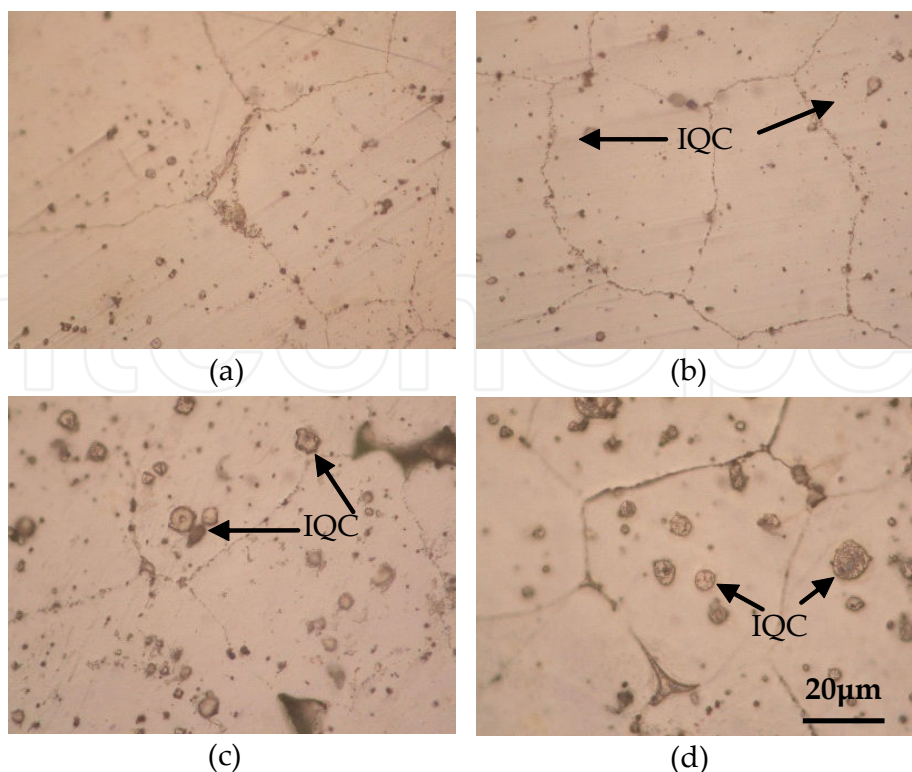


Figure 17. Microstructure of AZ91 alloys reinforced by different content of $Mg_{72}Zn_{25.7}Y_{1.5}Ce_{0.8}$ alloys after T4 solution treatment at 420C for 24h. (wt%) (a) 5% (b) 10% (c) 15% (d) 30%

After solution treatment (420C \times 24h), grain boundaries of AZ91 alloys became clear, the typical reticular morphology of β -phase disappeared, and I-phases and Al-Mn particles precipitated in the intragranular zone. It was difficult to distinguish between the two particles when the content of $Mg_{72}Zn_{25.7}Y_{1.5}Ce_{0.8}$ master alloy was low. I-phase was formed through the reaction of $L \rightarrow \alpha\text{-Mg} + I$ at about 400C during solidification process [10]. Therefore, under this temperature, small IQC particles increased in size and ripened during the long time process of T4 heat treatment. As shown in Fig.17, during the same heat treatment process, with the increase of $Mg_{72}Zn_{25.7}Y_{1.5}Ce_{0.8}$ alloy, the amounts and size of quaternary Mg-Zn-Y-Ce IQCs in AZ91 matrix gradually increased. The Al-Mn phases, however, did not change to bigger. This made the two kinds of particles distinguishable.

An aging treatment (220C \times 8h) was conducted after the solution treatment. With an aging temperature of 220C set between the continuous precipitation temperature (310C) and discontinuous precipitation temperature (150C), but nearer to the discontinuous precipitation temperature, the β -phases of AZ91 alloys mainly discontinuously precipitated. During the 8h aging treatment process, lamellar precipitates formed from the grain boundaries and grew in the intragranular. Granular β -phase also precipitated in the intragranular through a continuous precipitation method. Thus, precipitates filled the whole grain, as shown in Fig. 18.

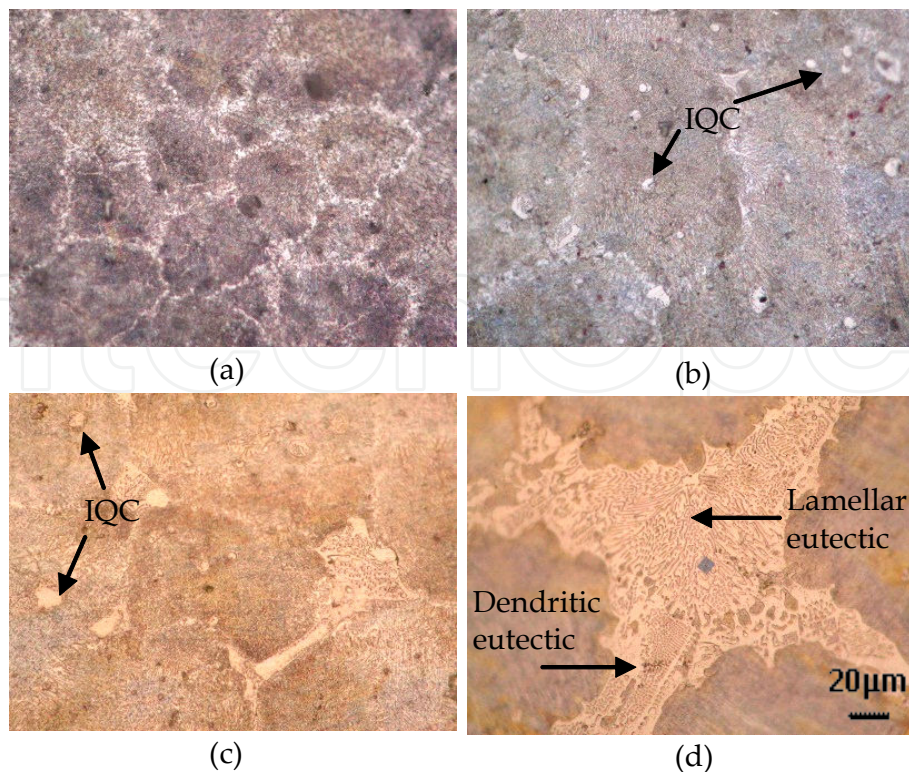


Figure 18. Microstructure of AZ91 alloys reinforced by different content of $Mg_{72}Zn_{25.7}Y_{1.5}Ce_{0.8}$ alloys after T6 solution(420Cx24h) and aging(220Cx8h) treatment. (wt%) (a) 5% (b) 10% (a) 15% (b) 30%

I-phase was difficult to be observed after the aging treatment when the content of $Mg_{72}Zn_{25.7}Y_{1.5}Ce_{0.8}$ alloy was small (5%). With an increase in the content of $Mg_{72}Zn_{25.7}Y_{1.5}Ce_{0.8}$ alloy, the amounts of IQCs in the grain of AZ91 alloys likewise increased. When the content of $Mg_{72}Zn_{25.7}Y_{1.5}Ce_{0.8}$ alloy continued to rise, the size of IQCs turned larger, but eutectic phases in grain boundaries became coarse. With the excessive addition of $Mg_{72}Zn_{25.7}Y_{1.5}Ce_{0.8}$ alloy, only a few I-phases remained in the intragranular AZ91 alloys; eutectic phases in the grain boundary became very thick, and the morphology of eutectic β -phase presented a lamellar. Meanwhile, parts of the eutectic α -Mg showed dendrite morphology.

Fig.19 shows that the value of the Brinell hardness (HB) of the IQC-reinforced AZ91 alloy decreased after the solution treatment, while its value remarkably increased after the further aging treatment. With the increasing addition of $Mg_{72}Zn_{25.7}Y_{1.5}Ce_{0.8}$ alloy, the HB values of as-cast and solution-treated AZ91 alloys showed a linear increase, while the HB values of aging-treated AZ91 alloys first increased and then decreased.

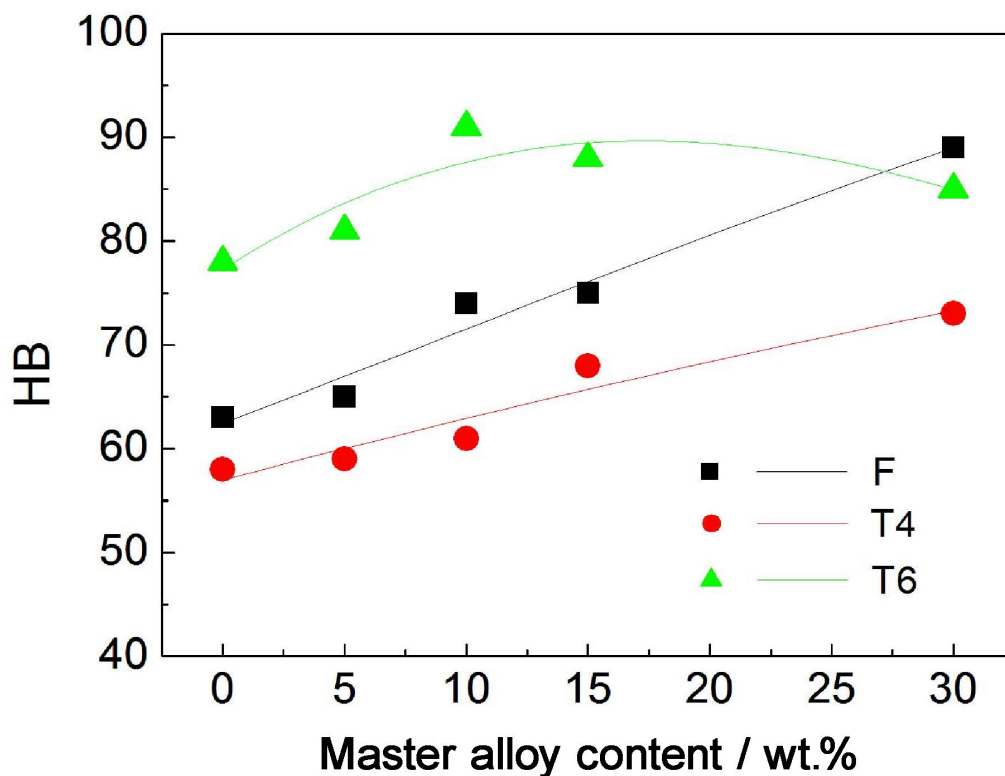


Figure 19. Relationship between additions of $Mg_{72}Zn_{25.7}Y_{1.5}Ce_{0.8}$ master alloy and Brinell hardness of AZ91 alloys.

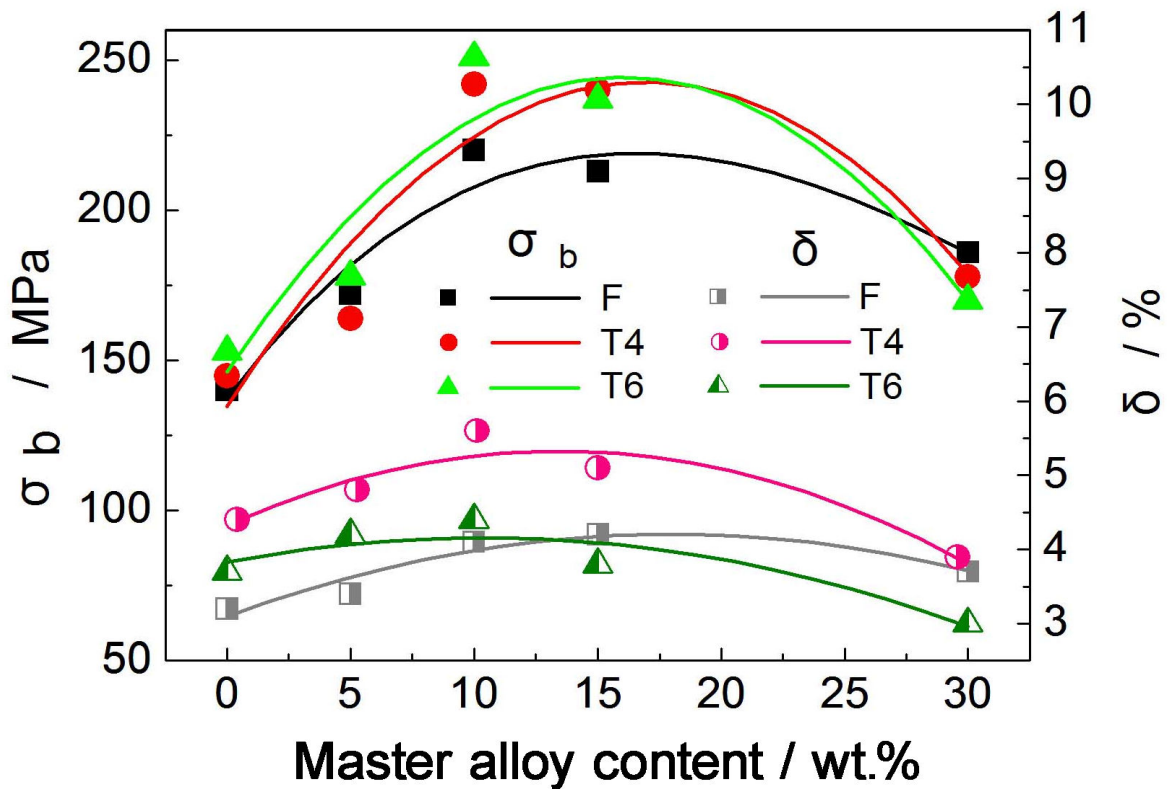


Figure 20. Relationship between additions of $Mg_{72}Zn_{25.7}Y_{1.5}Ce_{0.8}$ master alloy and mechanical properties of AZ91 alloys.

Fig.20 shows that the values of tensile strength (σ_b) and elongation (δ) of AZ91 alloys with all states reached their maximum when the content of $Mg_{72}Zn_{25.7}Y_{1.5}Ce_{0.8}$ alloy was about 10%. With increasing content of $Mg_{72}Zn_{25.7}Y_{1.5}Ce_{0.8}$ alloy, the mechanical properties of AZ91 alloys increased first and decreased subsequently.

After adding $Mg_{72}Zn_{25.7}Y_{1.5}Ce_{0.8}$ alloy into AZ91 alloys, the introduced Y and Ce elements played mixed roles in grain refinement and strengthening. Tensile strength and elongation of AZ91 alloys increased. Furthermore, a large number of introduced highly hardened IQC particles shifted the HB value of as-cast AZ91 and the value increased with the rising content of $Mg_{72}Zn_{25.7}Y_{1.5}Ce_{0.8}$ master alloy. The excessive addition of $Mg_{72}Zn_{25.7}Y_{1.5}Ce_{0.8}$ alloy reduced the mechanical properties of AZ91 alloys; these were related to the formation of coarse β -phase, which produced disordered effects to the matrix in the deformation process.

After the solution treatment, the majority of the main strengthening phase (reticulated β -phase) of AZ91 alloys disappeared, which made the HB value of solution-treated AZ91 alloys lower than in the as-cast. In addition, the microstructure of AZ91 alloys became homogeneous due to the annealing treatment. This eliminated most of the stress concentration and composition segregation. As a result, the tensile properties and plasticity of the heat-treated state AZ91 alloys showed small improvements compared to the as-cast AZ91 alloys. With additions of $Mg_{72}Zn_{25.7}Y_{1.5}Ce_{0.8}$ master alloy exceeding 10%, the reduced me-

chanical properties of AZ91 alloys resulted to large I-phases and dissevered effects to the matrix in the deformation process.

After the aging treatment, the lamellar eutectic β -phases that grew on the grain boundaries were parallel or perpendicular to the matrix; this played an important role in its strengthening. Due to the discontinuous precipitation of lamellar β -phases, with their main strengthening effect coming from this kind of precipitation method, in addition to continuous precipitation of pellet β -phases, the values of HB and tensile strength of AZ91 alloys rapidly increased. However, with the large amount of $\text{Mg}_{72}\text{Zn}_{25.7}\text{Y}_{1.5}\text{Ce}_{0.8}$ master alloy, the excess introduced a Y element, which brought about highly stable Al-Y phases during the aging treatment. These Al-Y phases resulted to a pinning effect on the nucleation and growth of β -phases, thereby preventing the precipitation of β -phases. Thus, the β -phases on the grain boundaries were very coarse and did not grow in the intragranular zone (as shown in Fig. 18(d)). Thick and hard β -phases can easily make cutting effects to the matrix. Their interfaces can easily be crack sources of the AZ91 alloys, which is unfavorable to the strength and plasticity of magnesium alloys. As a result, the tensile strength and elongation of AZ91 alloys decreased sharply.

4. Mg-based nano-quasicrystals [21,22]

In previous study [14~16, 19, 21~27], the effects of cooling conditions, heat treatment and the fourth components on QC morphology, size and volume fractions are detailedly researched. Spherical QCs with small size are fabricated in a relatively high cooling rate. In this part, we improve the cooling condition by using a water-cooled wedge-shaped copper mould (Fig. 21 shows its casting) to produce QCs in nanoscale.

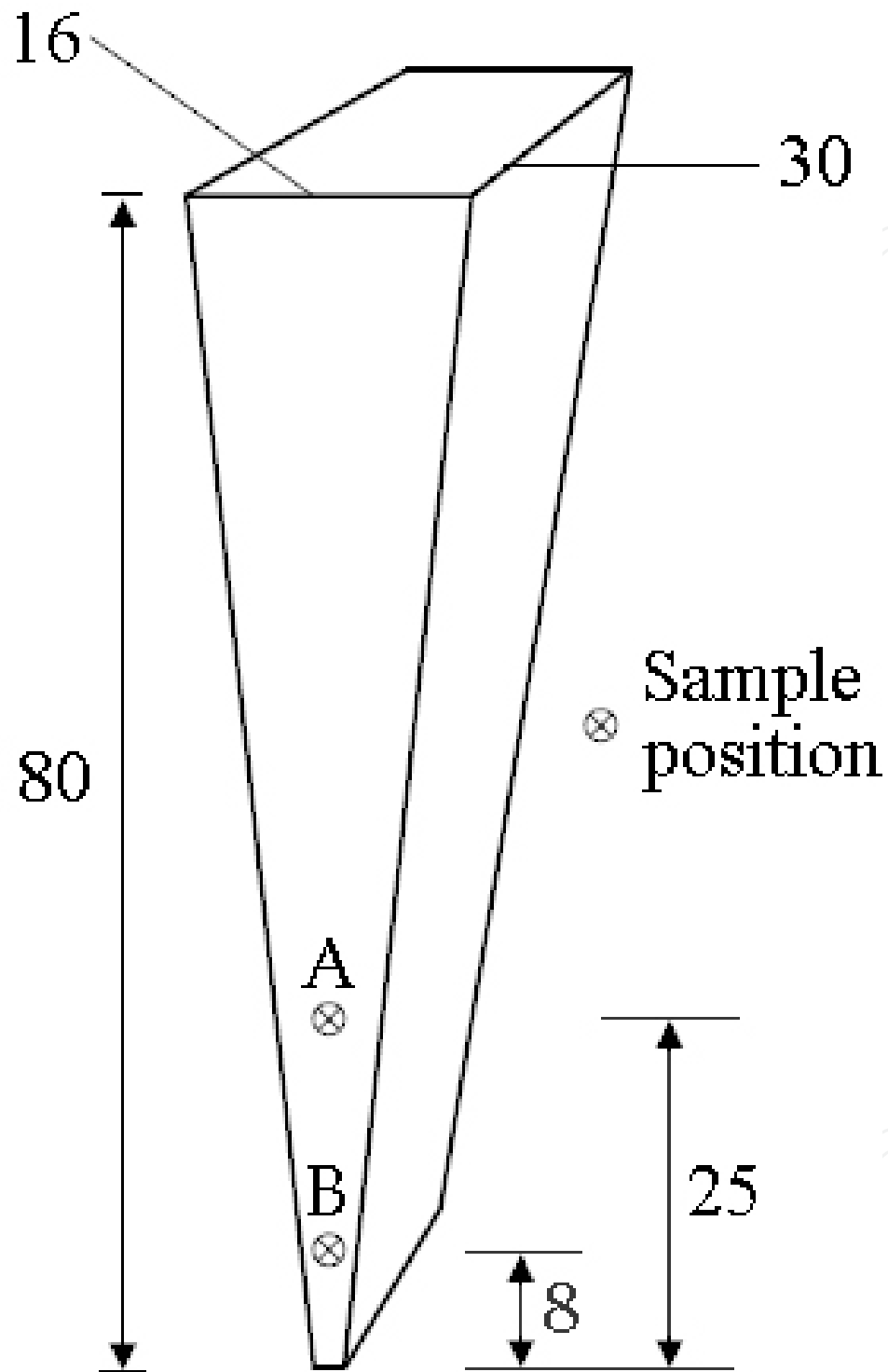


Figure 21. Sketch map of a wedge-shaped casting (mm)

TEM photos of QC alloys (Alloy compositions are listed in Table 3) in different sample positions are shown in Fig. 22. Three kinds of componential micro/nano QC phases are synthesized on tip of wedge-shaped castings. Energy-dispersive spectroscopy (EDS) analysis (Fig.

23) shows that micro/nano QC phases in Position B of Alloy 6 ~ Alloy 8 are Mg-Zn-Y phase,

Mg-Zn-Y-Cu phase and Mg-Zn-Y-Cu-Ni phase, respectively. The selected area electron dif-

fraction (SAED) patterns with typical five-fold rotational symmetry identify that these mi-

cro/nano QC phases are icosahedral QCs.

Alloy No.	Alloy compositions (at. %)				
	Mg	Zn	Y	Cu	Ni
6	72.0	26.0	2.0	-	-
7	71.0	26.0	2.0	1.0	-
8	71.0	26.0	2.0	0.5	0.5

Table 3. Nominal composition of the experimental alloys

Alloy No.	Sample position	QC size(diameter) / nm	QC morphology	Microhardness / HV
6	A	650-900	Petal-like	324
	B	330-340	Spherical	375
7	A	370-400	Spherical	367
	B	1.0-5.0	Spherical	459
8	A	20-55	Spherical	412
	B	8-30	Spherical	438

Table 4. Comparisons of the quasicrystals (QCs)

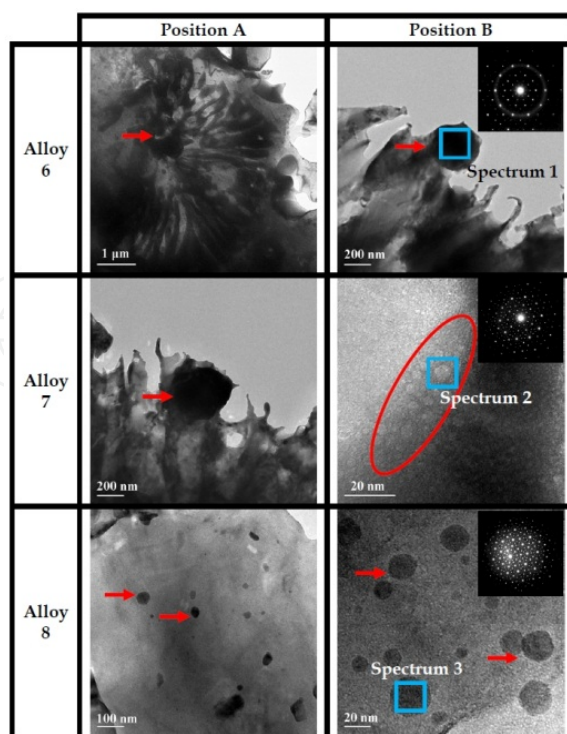


Figure 22. TEM photos of micro/nano-QC alloys and QC typical selected area electron diffraction (SAED) patterns on Position B of different alloys

Among all QCs, QCs in Position A of Alloy 6 show petal-like morphology, while others show spherical morphology. From the further analysis in Table 4, we can see that in alloys with same components, QCs in Position B are smaller than those in Position A, while QC microhardness in Position B is greater than that in Position A. After introducing Cu(-Ni) into Mg-Zn-Y alloys, we can see in the same sample position, QC size of Alloy 7 and Alloy 8 is obviously smaller than that of Alloy 6. QC size of Alloy 7 in Position A is close to that of Alloy 6 in Position B. Nano-QC spheres about 8~30 nm and 1~5 nm are synthesized in Position B of Alloy 8 and Alloy 7, respectively. It shows from the microhardness testing that the smaller the QC spheres, the greater their value of microhardness. Furthermore, the microhardness of nano-QC spheres in Position B of Alloy 7 exceeds HV450 which show fascinating properties.

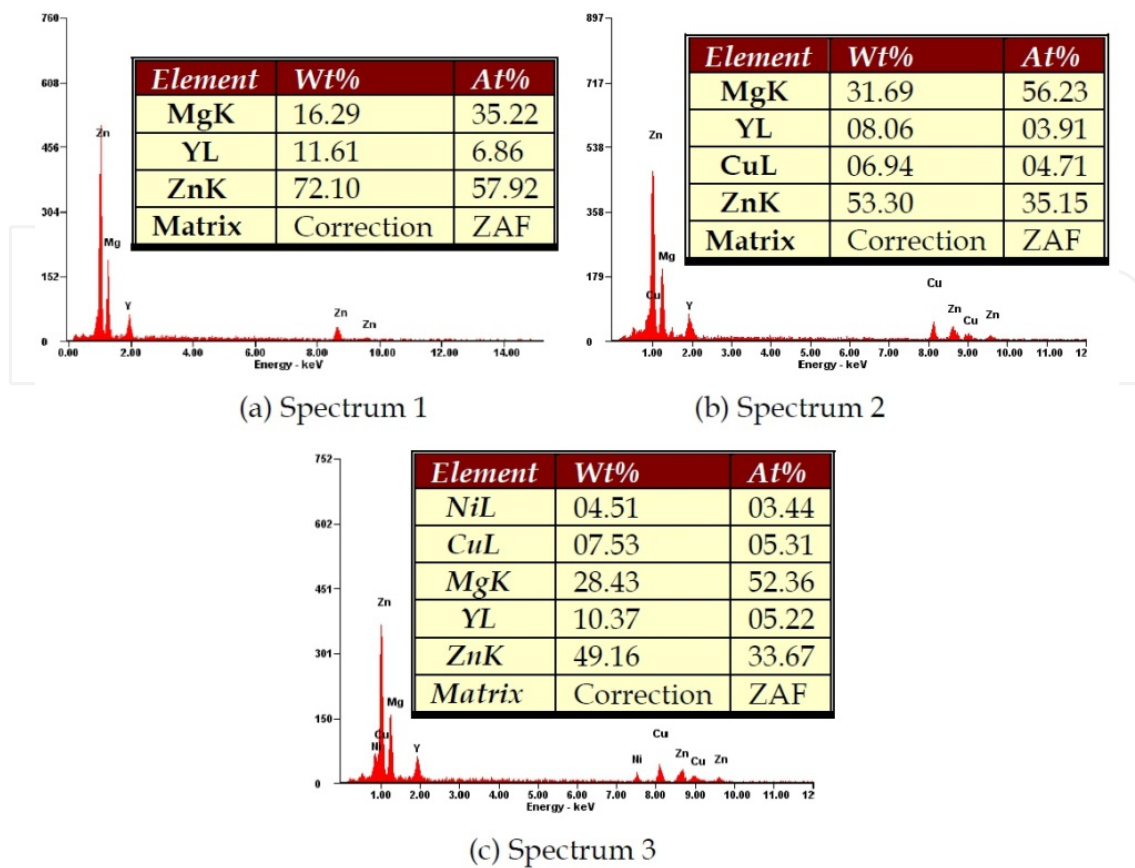


Figure 23. Energy-dispersive spectroscopy (EDS) analysis on QCs in Position B

Fig. 24 shows the potentiodynamic polarization curves of QC alloys (Position B) measured in simulated seawater open to air at room temperature. We can see that $Mg_{71}Zn_{26}Y_2Cu_1$ nano-QC alloy presents high corrosion resistance in simulated seawater and its corrosion resistance is much better than that of $Mg_{72}Zn_{26}Y_2$ and $Mg_{71}Zn_{26}Y_2Cu_{0.5}Ni_{0.5}$ QC alloys. The further study shows that this result can be ascribed to the existence of well-distributed nano-QC phases (shown in Fig. 25 by red arrows) and polygonal $Mg_2(Cu,Y)$ phases [28]. These high corrosion resistance phases decrease the anodic passive current density, improve the polarization resistance, cut down the corrosion rate (Table 5) and finally improve the corrosion resistance of the Mg-Zn-Y-based alloy markedly. Cu and Ni have long been considered as harmful elements for improving corrosion resistance of Mg-based alloy [29], however, they are used to synthesize nano-QC spheres in this paper. Due to high corrosion resistance of QC phases, $Mg_{71}Zn_{26}Y_2Cu_1$ and $Mg_{71}Zn_{26}Y_2Cu_{0.5}Ni_{0.5}$ nano-QC alloys present better corrosion resistance than $Mg_{72}Zn_{26}Y_2$ QC alloy. Moreover, the corrosion resistance of $Mg_{71}Zn_{26}Y_2Cu_1$ nano-QC alloys is higher than $Mg_{71}Zn_{26}Y_2Cu_{0.5}Ni_{0.5}$ nano-QC alloys for the higher damage level of Ni to the corrosion resistance of magnesium alloy than that of Cu when they have same contents [29].

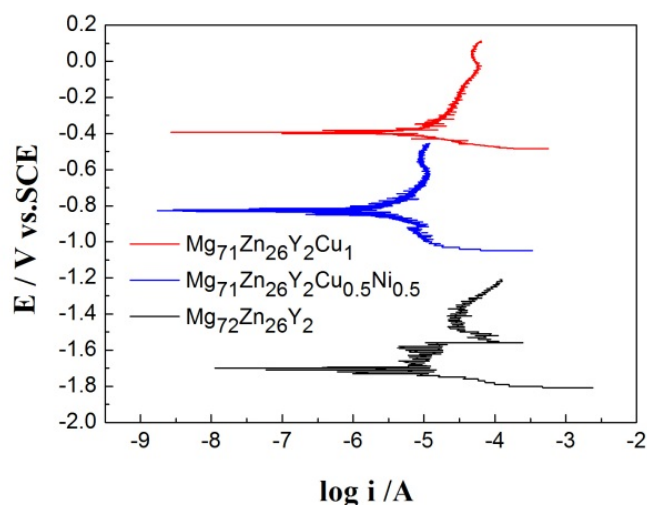


Figure 24. Potentiodynamic polarization curves of QC alloys (Position B) measured in simulated seawater open to air at room temperature

It was reported that a large negative enthalpy of mixing and/or existence of Frank-Kasper-type phases appear to be the crucial criteria for the formation of nanoquasicrystalline phase in any system [30]. Meanwhile, Mg-Zn-Y-based QCs just belong to Frank-Kasper-type phases [31] and have a certain negative enthalpy of mixing. So theoretically, Mg-Zn-Y-based nano-QCs can be formed in a proper cooling condition. The past cooling rate the researchers made to produce QCs was whether too high or too low, and was not content with the forming conditions of nano-QCs. This route just meets the demands for forming nanoscale QCs. So, nano-QCs are successfully produced in this paper. Moreover, the additions of Cu and Ni improve the degree of constitutional supercooling of Mg-Zn-Y melts and reduce the crucial criteria radius for forming spherical QCs. However, increasing thermodynamics undercooling coming from water-cooled wedge-shaped copper mould make it still possible to form spherical QCs. At the same time, the alloy components designed for this study is based on the three empirical rules [32] for the formation of metallic glass. It has been widely accepted that quasicrystals and at least some metallic glasses are built up with icosahedral clusters [33]. The short-range atomic configuration is very similar between the quasicrystal and amorphous phases [34]. On the tip of the wedge-shaped ingots, its cooling conditions are just suitable for these icosahedral clusters to be nucleation of QCs. And then, it leaves very short time for quasicrystal growth. So, it is nano-QCs that form in this route instead of metallic glasses.

Specimen	$i_{\text{corr}}/\mu\text{A}/\text{cm}^2$	$R_p/\text{k}\Omega$	Corrosion Rate/mpy
6#	11.09	6.925	19.298
7#	2.035	14.76	1.522
8#	3.762	8.105	3.084

Table 5. Corrosion parameters obtained from potentiodynamic polarization curves for Position B of QC alloys in simulated seawater. I_{corr}: corrosion current; R_p: polarization resistance.

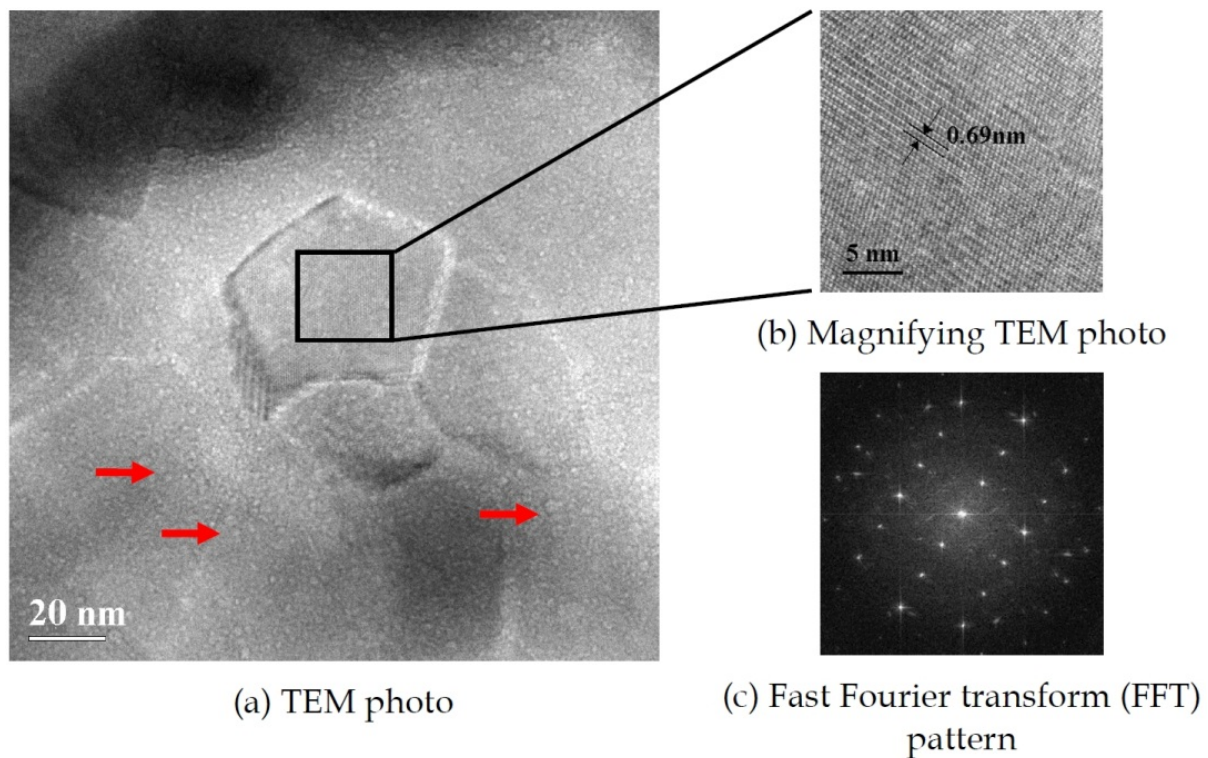


Figure 25. Pentagonal nanophase in Mg₇₁Zn₂₆Y₂Cu₁ alloy

5. Summary

The existing results show that QC characteristics are influenced by the cooling conditions during QC nucleation and subsequent growth. In macroscopic view, transformations of QCs in morphology, size and volume fractions are caused by changes of the cooling rate, the additions of fourth components and heat treatments. The further theoretical research shows that the final morphology of a QC determined by the critical stable radius R_c . Only when the real radius of a QC less than R_c can spherical IQC be formed. Otherwise, petal-like QCs will form.

QC master alloys can be used to strengthen magnesium alloys. Proper doses may induce an improvement in mechanical properties of a magnesium alloy. Furthermore, we can fabricate nano-QCs by controlling thermodynamics undercooling and using a water-cooled wedge-shaped copper mould. Due to the good corrosion resistance of QCs, nano-QCs containing magnesium alloy show higher corrosion resistance.

Although QCs have been studied for about 30 years by scientists all over the world, successful applications of QCs have been very limited. For example, QCs can be applied as a sur-

face coating for frying pans, could be used in surgical blades, and could be incorporated into hydrogen storage materials [2]. These are insufficient to meet people's demand for this amazing material. New applications are expected to develop.

Acknowledgement

We are grateful for the financial support of the Natural Science Foundation of Hebei Province, China (No. E2010000057, No. E2010000121) and the International Science & Technology Cooperation Program of China (No. 2010DFA51850).

Author details

Zhifeng Wang and Weimin Zhao*

School of Materials Science and Engineering, Hebei University of Technology,, P. R. China

References

- [1] Levine, D., & Steinhardt, P. J. (1986). Quasicrystals. I. Definition and Structure. *Physical Review B*, 1098-0121, 34, 596-616.
- [2] Louzguine-Luzgin, D. V., & Inoue, A. (2008). Formation and Properties of Quasicrystals. *Annual Review of Materials Research*, 1531-7331, 38, 403-423.
- [3] Shechtman, D., Blech, I., Gratias, D., & Cahn, J. W. (1984). Metallic Phase with Long-range Orientational Order and No Translational Symmetry. *Physical Review Letters*, 0031-9007, 53, 1951-1953.
- [4] Patricia, T. (2007). Quasicrystals- When All Pieces Fit Together. *Nature Materials*, 1476-1122, 6, 11-12.
- [5] Tsai, A. P., Inoue, A., & Masumoto, T. (1989). Stable Decagonal Al-Co-Ni and Al-Co-Cu Quasicrystals. *Materials Transactions*, 1345-9678, 30, 463-473.
- [6] Luo, Z. P., Zhang, S. Q., Tang, Y. L., & Zhao, D. S. (1993). Quasicrystals in As-cast Mg-Zn-RE Alloys. *Scripta Metallurgica et Materialia*, 0095-6716X., 28, 1513-1518.
- [7] Bindi, L., Steinhardt, P. J., Yao, N., & Lu, P. J. (2009). Natural Quasicrystals. *Science*, 0036-8075, 324, 1306-1309.
- [8] Bindi, L., Eiler, J. M., Guan, Y. B., et al. (2012). Evidence for the Extraterrestrial Origin of a Natural Quasicrystal. *Proceedings of the National Academy of Sciences of the United States of America (PNAS)*, 0027-8424, 109, 1396-1401.
- [9] Blaaderen, A. V. (2009). Quasicrystals from Nanocrystals. *Nature*, 0028-0836, 461, 892-893.

- [10] Zhang, Y. B., Yu, S. R., Zhu, X. Y., & Luo, Y. R. (2008). Study on As-cast Microstructures and Solidification Process of Mg-Zn-Y Alloys. *Journal of Non-Crystalline Solids*, 0022-3093, 354, 1564-1568.
- [11] Anderson, B. C., Bloom, P. D., Baikerikar, K. G., et al. (2002). Al-Cu-Fe Quasicrystal/Ultra-high Molecular Weight Polyethylene Composites as Biomaterials for Acetabular Cup Prosthetics. *Biomaterials*, 0142-9612, 23, 1761-1768.
- [12] Schwartz, C. J., Bahadur, S., & Mallapragada, S. K. (2007). Effect of Crosslinking and Pt-Zr Quasicrystal Fillers on the Mechanical Properties and Wear Resistance of UHMWPE for Use in Artificial Joints. *Wear*, 0043-1648, 263, 1072-1080.
- [13] Abe, E., Yan, Y., & Pennycook, S. J. (2004). Quasicrystals as Cluster Aggregates. *Nature Materials*, 1476-1122, 3, 759-767.
- [14] Wang, Z. F., Zhao, W. M., Li, H. P., et al. (2011). Morphologies of Quasicrystal Phase in Ternary Mg-Zn-Y Alloys. *Materials Science Forum*, 0255-5476, 675-677, 215-218.
- [15] Wang, Z. F., Zhao, W. M., Hur, B. Y., et al. (2009). Effects of the Fourth Component and Undercooling on Morphology of Primary Mg-Zn-Y Icosahedral Quasicrystal Phase under Normal Casting Conditions. *China Foundry*, 1672-6421, 6, 293-299.
- [16] Wang, Z. F., Zhao, W. M., Li, H. P., et al. (2010). Effect of Titanium, Antimony, Cerium and Carbon Nanotubes on the Morphology and Microhardness of Mg-based Icosahedral Quasicrystal Phase. *Journal of Materials Science & Technology*, 1005-0302, 26, 27-32.
- [17] Zhang, J. S., Du, H. W., Liang, W., Xu, C. X., & Lu, B. F. (2007). Effect of Mn on the Formation of Mg-based Spherical Icosahedral Quasicrystal Phase. *Journal of Alloys and Compounds*, 0925-8388, 427, 244-250.
- [18] Mullins, W. W., & Swkerka, R. F. (1963). Morphological Stability of a Particle Growing by Diffusion or Heat Flow. *Journal of Applied Physics*, 0021-8979, 34, 323-329.
- [19] Wang, Z. F., Zhao, W. M., Li, H. P., et al. (2010). Fabrication of Quaternary Mg-Zn-Y-Ce Quasicrystal Alloys and Their Strengthening Effects on AZ91 Magnesium Alloys. *China Foundry*, 1672-6421, 7, 342-348.
- [20] Zhang, J. S., Pei, L. X., Du, H. W., Liang, W., Xu, C. X., & Lu, B. F. (2008). Effect of Mg-based Spherical Quasicrystals on Microstructure and Mechanical Properties of AZ91 Alloys. *Journal of Alloys and Compounds*, 0925-8388, 453, 309-315.
- [21] Wang, Z. F., Zhao, W. M., Qin, C. L., et al. (2012). Direct Preparation of Nano-Quasicrystals via a Water-Cooled Wedge-Shaped Copper Mould. *Journal of Nanomaterials*, Article ID 708240, 1687-4110, 2012
- [22] Wang, Z. F., Zhao, W. M., Qin, C. L., & Cui, Y. (2012). Fabrication and Corrosion Resistance of Mg-Zn-Y-based Nano-quasicrystals Alloys. *Materials Research*, 1516-1439, 15, 51-56.

- [23] Wang, Z. F., Zhao, W. M., Lin, X. P., et al. (2009). Effect of Mn and Cu on Spheroidized Process of Mg-Zn-Y-based Icosahedral Quasicrystal Phase. *Advanced Materials Research*, 1022-6680, 79-82, 1403-1406.
- [24] Wang, Z. F., Zhao, W. M., Li, H. P., et al. (2011). Effects of Cooling Rate on Morphology, Microhardness and Volume Fraction of Mg-Zn-Y Quasicrystals. *Advanced Materials Research*, 1022-6680, 160-162, 470-474.
- [25] Wang, Z. F., Zhao, W. M., Li, H. P., et al. (2011). Heat Treatment and Morphology Study of Mg-Zn-Y Quasicrystal Alloys. *Advanced Materials Research*, 1022-6680, 189-193, 3824-3827.
- [26] Wang, Y. M., Wang, Z. F., Zhao, W. M., et al. (2011). Effects of Cooling Rate on Quasicrystal Microstructures of Mg-Zn-Y Alloys. *Advanced Materials Research*, 1022-6680, 160-162, 901-905.
- [27] Zhao, W. M., Wang, Z. F., Li, H. P., et al. (2011). Thermodynamics and Dynamics Study on Solidification Process of Mg₃Zn₆Y quasicrystals. *Advanced Materials Research*, 1022-6680, 214, 128-132.
- [28] Zhang, J., Qiu, K., Wang, A., et al. (2004). Effects of Pressure on the Solidification Microstructure of Mg₆₅Cu₂₅Y₁₀ Alloy. *Journal of Materials Science & Technology*, 1005-0302, 20, 106-108.
- [29] Song, G. L. (2006). *Corrosion and Protection of Magnesium Alloys*, Chemistry Industry Press, 978-7-50258-565-5 Beijing, China. (In Chinese)
- [30] Murty, B. S., & Hono, K. (2004). On the Criteria for the Formation of Nanoquasicrystalline Phase. *Applied Physics Letters*, 0003-6951, 84, 1674-1676.
- [31] Sterzel, R., Dahlmann, E., Langsdorf, A., & Assmus, W. (2000). Preparation of Zn-Mg-Rare Earth Quasicrystals and Related Crystalline Phases. *Materials Science and Engineering A*, 0921-5093, 294-296, 124-126.
- [32] Inoue, A. (2000). Stabilization of Metallic Supercooled Liquid and Bulk Amorphous Alloys. *Acta Materialia*, 1359-6454, 48, 279-306.
- [33] Dong, C., Chen, W., Wang, Y., et al. (2007). Formation of Quasicrystals and Metallic Glasses in Relation to Icosahedral Clusters. *Journal of Non-Crystalline Solids*, 0022-3093, 353, 3405-3411.
- [34] Inoue, A., Tsai, A. P., Kimura, H. M., & Masumoto, T. (1988). Enthalpy Relaxation Behaviour of Al-Si-Cr Quasicrystalline and Amorphous Alloys upon Annealing. *Journal of Materials Science*, 0022-2461, 23, 429-437.